Millisecond, Microsecond, Nanosecond: What Can We Do With More Precise Time?

Edmund O. Schweitzer, III, David E. Whitehead, Greg Zweigle, Veselin Skendzic, and Shankar V. Achanta,
Schweitzer Engineering Laboratories, Inc.

***Abstract*—Our industry moves energy at the speed of light, at the flick of a switch. A transmission line transporting 1500 megawatts delivers the equivalent of 250 pounds of coal per second, already converted into a convenient form of energy. For decades, we considered time in seconds or cycles: such as fuse curves and breaker clearing times. About three decades ago, our thinking moved into milliseconds because we needed to get better at quickly understanding wide-area events, protection was getting faster allowing for more power transfer, and the technology made it possible. Over the past decade, we have come to appreciate how synchrophasors can help us understand, control, and protect our power systems. One electrical degree at 60 hertz is about 46 microseconds, so measurements accurate to ten microseconds give us accurate synchrophasors. Traveling-wave technologies can put nanosecond resolution to good use. Achieving nanosecond absolute time is practical, affordable, and useful. In this paper, we explore how more-accurate time can improve the performance of electric power systems.**

I. Introduction

"The only reason for time is so that everything doesn't happen at once."—Albert Einstein.

Time helps us order and organize events. Early time sources were celestial and based on astronomic observations. Time was local: linked directly to the observer's geographic location. It took many centuries until maritime and railroad travel encouraged globally standardized time. Increasingly precise timekeepers (mechanical clocks) often had to be transported between locations in order to synchronize clocks.

This paper reviews time as it has been used in power system applications and the associated advancements that have yielded improved performance. It then describes power system timing technologies, discusses methods for maintaining absolute time in the event of a lost external timing reference, and finally introduces advanced applications that are becoming available and reliable.

II. A Review of Time as It Relates to the Power System

At the turn of the 20th century, the telegraph, followed shortly thereafter by wireless communications, provided a low-cost, wide-area method to distribute time. The power system joined the effort in the 1930s with the invention of the Hammond electric clock, Fig. 1.

The Hammond clock took advantage of the stable power system frequency to drive a synchronous motor that brought accurate time into every household. The clock allowed power companies to provide both energy and accurate time. The power system became the first wide-area time-synchronization system that everyone could afford.

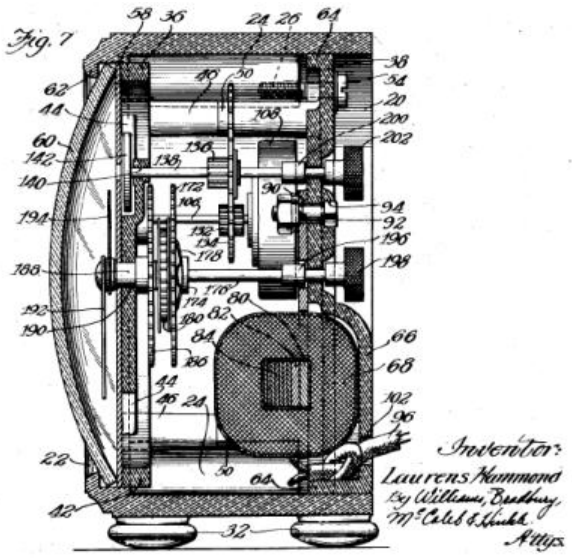

Fig. 1. Hammond Electric Clock.

A. Prior to 1960: No Time Reference for Protection

Prior to the 1960s, time was not explicitly used in power system protection. Electromechanical relays could not benefit from external timing signals [1]. Relay measurements were local and did not require time synchronized information from other locations.

B. 1960 to 1980: Seconds

In the 1960s, supervisory control and data acquisition (SCADA) systems brought data from various locations in the power system to a centralized location so that operators could ascertain the state of the power system and perform direct control [2]. SCADA scans were, and still are, in the order of seconds.

C. 1980 to 2000: Milliseconds

As protection moved into the digital age, and with the inclusion of precise time protocols such as IRIG-B, accurate time became an important attribute of managing the power system. One of the authors incorporated IRIG-B time-code clock synchronization in a digital relay in 1985. Time-stamped information from digital relays, such as oscillography and sequential event records, provided valuable information and insight into the operation of the power system. Relays were now providing millisecond time-stamped information. As early as

1985, system fault locating using traveling waves and precise time was developed and deployed [3].

D. 2000 to 2012: Microseconds

A decade ago, new technology took advantage of GPS and enabled wide-area measurements of faster changing signals, such as phase angles. One electrical degree, at 60 hertz, is 46 microseconds. Measuring and comparing phase angles to a quarter degree accuracy was desired and required timing accuracy and precision of at least 10 microseconds. In order to give allowance for other sources of error, the actual time accuracy and precision were provided to within one microsecond. The ability to measure with microsecond accuracy allowed the development of synchrophasor systems for applications ranging from visualization to real-time control [4] [5].

At the wide-area visualization and analysis level, direct sampling of analog waveforms with microsecond time stamps was in development [6]. This enabled shifting of the signal processing burden from the measuring devices to the applications. Instead of computing synchronized phasors at the measuring devices and transmitting them to an application for consumption, the application computes them directly. This enabled a single measuring device to serve a wider range of applications.

E. 2012 and Looking Forward: Nanoseconds

With improvements in computational power, precise time sources, and communications systems, we have taken a fresh look at traveling-wave technologies and applications. Recently, we have applied the traveling-wave principles to fault location and protection [7]. Traveling-wave technologies require nanosecond accuracy and precision.

III. Relevance of Time to Power System Protection

Let's look at signal measurement technologies as a function of sampling rate. Then we will quantify the relationship between measurement and time accuracy, for both today's and emerging signal-measurement systems.

A. Phasor-Based Measurements: Quasi-Stationary Constraint

Both SCADA and synchrophasors generally assume signals are quasi-stationary [8]. The quasi-stationary approximation works well because during steady-state stationary operation, signals on the power system are sinusoidal with a peak value a, frequency f, and phase offset θ as shown in (1).

$$x(t) = a\ cos(2\pi ft + \theta) \tag{1}$$

In steady state, the quantity $x(t)$ is represented mathematically by a phasor quantity $\vec{X}$ with no time dependence as shown in (2), where $A = a/\sqrt{2}$.

$$\vec{X} = A\ exp(j\theta) \tag{2}$$

The stationary phasor representation is extremely powerful for analysis of systems operating at steady-state and at a single frequency. The quasi-stationary approximation keeps this phasor representation while including a limited amount of time dependence. This approximation is valid when measured power system quantities are changing more slowly than the bandwidth of the measurement system. Consider the case of slow magnitude variations, $A(t)$, and slow frequency variations, $\Delta f(t)$. Define $\Delta f(t)$ as referenced to a fixed nominal frequency f_{nom}.

$$f = f_{nom} + \Delta f(t) \tag{3}$$

The phasor relationship (2) becomes a function of time through these slow amplitude and frequency variations.

$$\vec{X}(t) = A(t)\ exp\left(j\left[\int_0^t 2\pi\Delta f(\sigma)d\sigma + \theta\right]\right) \tag{4}$$

The quasi-stationary approximation results in filtering that tracks and selects the fundamental frequency component of the measured signal, along with a small bandwidth of signal surrounding that fundamental component.

SCADA systems traditionally acquire data at rates of one sample per second or lower. Communication of measured values is based on polling that does not typically include a time stamp. The top portion of Fig. 2 shows a power system event as measured by a SCADA system sampling once per second. There appears to be a slight increase in the current magnitude of the signal at approximately four seconds. After this, the magnitude goes to zero. It is difficult to determine the exact conditions of the power system or the cause of this magnitude change from SCADA. However, the SCADA measurements are able to communicate that the current decreased to zero at around five seconds. This information is useful for identifying an open circuit in the power system.

Synchrophasor systems acquire data at rates ranging from 30 samples per second to as high as 240 samples per second, and they include the phase angle. The bottom portion of Fig. 2 shows the same event as measured by synchrophasors. For ease of comparison only the magnitude of the signal, not the phase angle, is shown in the synchrophasor chart. From the synchrophasor data, a slightly better understanding of the system change is possible.

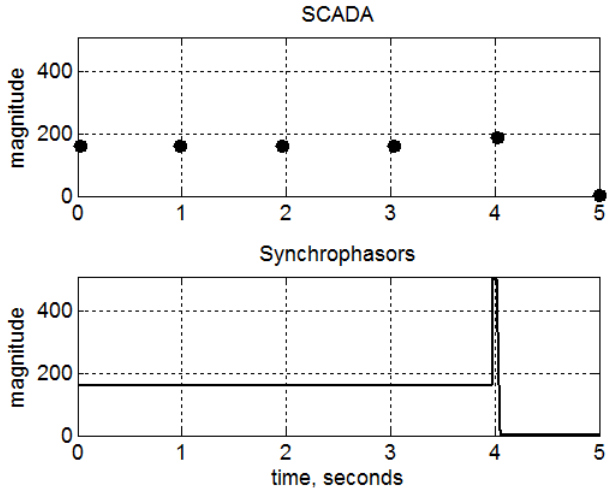

Fig. 2. Power system event as seen by SCADA and synchrophasor measurement technologies. The vertical axis is the current magnitude in amperes.

B. Direct Time-Based Measurements

Moving beyond the quasi-steady state phasor approximation are applications that directly sample power system signals at

full bandwidth. For example, modern event reports use sample rates in the range of 400 to 8,000 samples per second. Many can record the original waveforms without any conversion to phasors.

Event reports record power system data. Like synchrophasors, modern event reports use a common, precise time reference, such as GPS. It is also possible to measure and stream data at rates comparable to event reports. Typical examples of this approach include line current differential schemes [9], the substation-wide sampled values streaming with data formatted in accordance to IEC 61850-9-2 [10] [11], and wide-area streaming formatted in accordance to IEC 61850-90-5 or IEEE C37.118.2 [12].

With direct time-domain sampling of analog waveforms using a common precise time reference, it is possible to move application-dependent signal processing from the measuring device to the applications themselves. A prototype of a wide-area wide spectrum (WWS) system has been deployed at three sites across North America [6]. This demonstration system samples at 1,200 samples per second and requires 350 kbps per device to communicate the data over a wide area. Applications perform time-alignment between multiple streams at the receiving side.

We are developing devices that sample and communicate measurements at millions of samples per second or faster [7]. The devices use a very high-accuracy time source to time-stamp the data. Fig. 3 shows the same event as in Fig. 2, except with time-domain data acquisition and display methods. For clarity, we have localized the time range around the disturbance at four seconds. Clearly, there is a significant increase in the information content when going from SCADA to synchrophasors and then from synchrophasors to time-domain high-rate signal sampling.

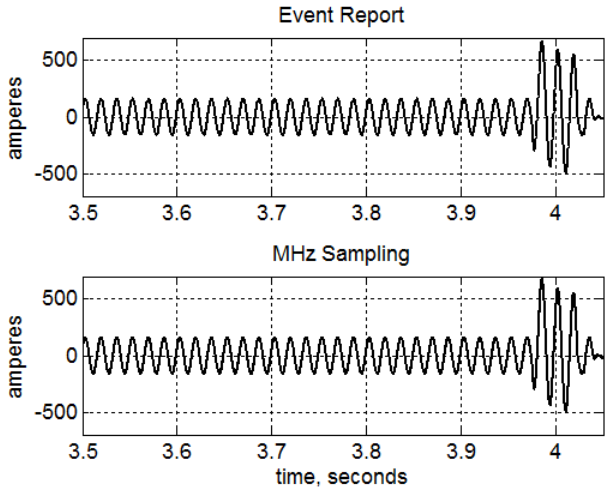

Fig. 3. Time-aligned power system event as seen at 8,000 samples per second (event report rates) and 1.5 million samples per second.

When we go from 8,000 samples per second (top portion of Fig. 3) to 1.5 million samples per second (bottom portion of Fig. 3) they appear identical. When we examine a shorter time window that is positioned at the leading edge of the fault event, we see traveling waves in the fast-sampled data but not in the traditional event report.

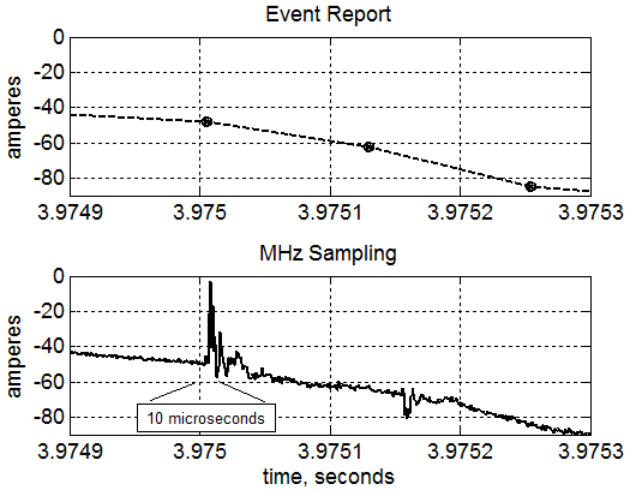

Fig. 4. A traveling wave is only visible at the higher sampling rate. The dashed line connecting the sample points in the event report is for visual comparison only. No measured values are between these sample points.

Table I shows a range of applications, along with their sampling rate and time accuracy.

TABLE I
POWER SYSTEM TIMING ACCURACY REQUIREMENTS

Application	Sampling Rate	Time Accuracy
SCADA	0.2–1 Hz	0.2–1 s
Event reporting	0.4–8 kHz	10 µs–1 ms
Synchrophasors	30–240 Hz	1–23 µs
WWS	1–5 kHz	1–10 µs
Traveling-wave fault location	1–2 MHz	100–500 ns
Lightning detection	1–2 MHz	100–500 ns
Medium voltage distribution monitoring	1–5 MHz	40–100 ns
Partial discharge source identification	> 5 MHz	10–50 ns

IV. TIME-KEEPING METHODS, PROTOCOLS, AND SYSTEMS FOR ELECTRIC POWER SYSTEMS

A. Clocks

Today, when we hear "precise time," GPS clocks are almost always the first things to come to mind. They offer absolute accuracy around the world. We are achieving absolute accuracies in the tens of nanoseconds, with high-quality, affordable, easy-to-use GPS clocks that pick up the radio-frequency signals from satellites. This state-of-the-art accuracy and affordability are desirable and suitable for use even in small substations, recloser cabinets, and at tap changer controls. However, GPS timing is not guaranteed for the following reasons:

- The U.S. government owns and operates the GPS system and can deny and degrade the services at will. For example, from time to time, the U.S. government issues NOTAMS (notices to airmen) indicating dates, times, and areas where GPS will not be reliable.

- Naturally occurring events, such as solar flares, can knock out GPS service for minutes at a time.
- The satellite signals are relatively weak, making them easy to jam and spoof. This causes either the loss of precise time or the time from the GPS clocks to be driven off of the true and absolute time.
- Clocks and timing systems can experience hardware failures, human error, etc.

As always in protection and control, we must consider failure modes and their consequences and mitigate them. Disciplined standards "lock" to good time, once locked, aren't "pulled off" by bad time, and "keep on ticking" with very low drift rates. Disciplined clocks can be a part of robust time distribution systems. In well-designed time systems, it is possible to detect and discard the bad time, say from a GPS receiver, and rely on the disciplined standard for a very long time before clock drift becomes an issue. Alternate time sources that are available to validate GPS include wide-area radio frequency (RF) and terrestrial time sources. The authors believe there may be value in reconsidering clock receivers that use the Very Low Frequency (VLF) transmissions from stations such as WWVB at 60 kilohertz. We believe time precision and accuracy on the order of 100 microseconds to 1 millisecond may be attainable. Terrestrial time distribution over fiber is another solution that we cover later in this section.

One commercially-available clock [13] simultaneously receives time signals from two satellite constellations: GPS (U. S.) and GLONASS (Russian). The clock then compares these two time values, and, if they are not within certain limits, the clock produces a signal to inform time users of potential problems. This security capability doubles defense against jamming and spoofing.

Hiding and protecting GPS antennas from observation and jamming and spoofing can also help. Mounting the GPS antennas up high, concealing them from easy observation from the ground, and shielding them from terrestrial noise, jamming, and spoofing signals are good design practice.

Regardless of the clock used, power system designers must take into account what happens when time is lost. This is not much different than a protection engineer considering what happens when a pilot-protection channel goes down. We must gracefully fall back to possibly degraded performance. We can't get accurate synchrophasors over the wide area if the clock is not accurate, and protection will be slower if the pilot channel fails.

Beginning with time sources, such as clocks and time-division multiplexed networks, and using the time-verification devices, we can build single and redundant time-distribution systems. These systems deliver precise time into the nanoseconds throughout entire generating stations, wind farms, solar farms, substations, factories, and office buildings. These time-distribution systems are independent of computer networks. Fig. 5 depicts a time distribution system that achieves reliability and dependability for precise time distribution in a power system.

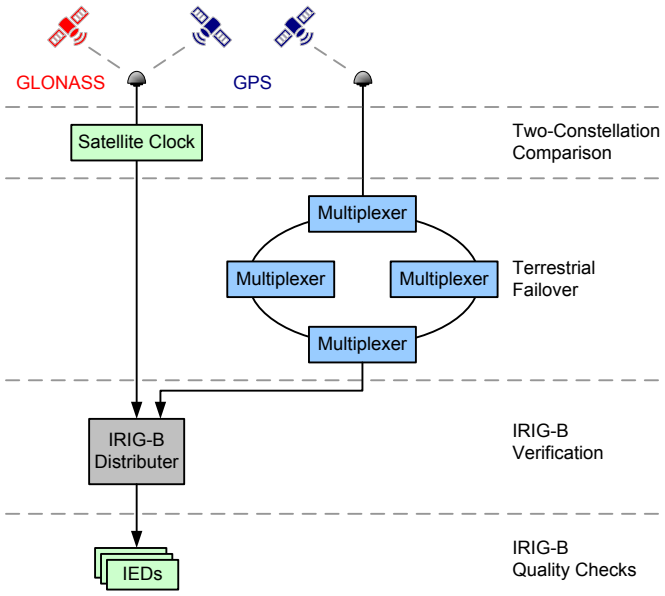

Fig. 5. Reliable and dependable time distribution system.

Reference [14] describes a device that accepts two sources of IRIG-B time code, compares them for accuracy, and evaluates their time quality bits. To detect spoofing and deal with jamming, the device compares two IRIG-B signals and associated quality bits and uses a patented process to determine time coherency. The device also can distribute time to a large number of relays, meters, and other equipment. Because the referenced device has a phase-locked loop, it is able to regenerate demodulated IRIG-B signals when external GNSS signals are not present and remove the propagation delays due to cabling.

B. Distribution of Time Over Wide Areas

Today, wide-area fiber-optic communications systems are distributing precise time to the tens of nanoseconds. Reference [14] describes the only terrestrial time distribution known to the authors at this time. It is a time-division multiplexed system that clocks data synchronously. Leveraging the communications protocol synchronism requirement makes it very practical to use as a wide-area time reference. All nodes to the communications system are synchronized to the same reference to within one microsecond. This reference can be a source of absolute time, such as GPS, with a disciplined clock for backup; see Fig. 6. Even *if* the GPS were to be spoofed successfully, it doesn't affect applications associated with this communications system, because all nodes remain synchronized.

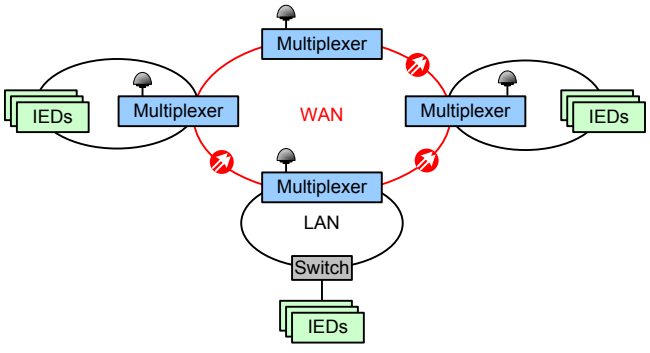

Fig. 6. Wide-area fiber-optic time distribution network.

When Bonneville Power Administration (BPA) was pioneering traveling-wave fault locating technology, they initially used their wide-area microwave communications system to convey surge-arrival times. They identified the traveling-wave arrival time by putting a trigger pulse on the baseband of the microwave system. We can use similar techniques by using fiber to communicate an instant in time between stations.

The communications channels for current-differential protection offer another opportunity to convey time. The VLF radio signals mentioned in the preceding section are still one more opportunity, but at lesser accuracy. Timing communicated via a private network using the Network Time Protocol (NTP), described later, is typically limited to one to two milliseconds of accuracy. Still less accurate and much less dependable is NTP over a public network such as the Internet. The authors do not recommend implementing time-distribution systems over a public network.

As of today, the best way to deliver time to the tens of nanoseconds over wide areas is a time-division multiplexer system referenced to a GPS satellite clock capable of using both satellite constellations.

C. IRIG-B Time Code

This time code was introduced in 1960, by the Inter-Range Instrumentation Group, part of the U. S. Department of Defense. The problem being addressed was synchronizing clocks at various satellite and missile tracking stations around the world, so that the telemetry and radar tracks could be integrated nicely. The time signal was initially a one kilohertz carrier, conveying a 100-pulse per second pulse-width-modulated code. "On" is represented by 100 percent modulation of the one kilohertz signal, and "off" is represented by 50 percent. Pulse widths of two, five, and eight milliseconds represent zero, one, and framing, respectively. Each pulse period is ten milliseconds, so one frame is one second. Pulses contained either two, five, or eight cycles of the kilohertz carrier at full modulation level, and the carrier is always present.

IRIG-B is easy to generate, understand, and decode. It has been distributed over telephone wire, coaxial cables, fiber, microwave, high frequency, and other radio channels and recorded alongside telemetry and radar data. If you record it on an oscillogram, you can easily decode its binary-coded-decimal representation of time. Accuracy is limited only by one's ability to determine the phase of the one kilohertz carrier accurately.

Another form of IRIG-B is so-called "demodulated" IRIG-B. There is no carrier, only the two, five, and eight millisecond pulses every ten milliseconds. Because this time code has a sharp edge every ten milliseconds, time clocks generating demodulated IRIG-B can produce 100 edges per second on the ten-millisecond mark, and offer accuracies in the tens of nanoseconds per edge. Devices using demodulated IRIG-B can use phase-locked loops to track and average these edges to produce internal time references locked to the external source for nanosecond accuracy. Time-quality bits were added to inform the user how far the clock may have drifted from absolute time.

Keep in mind that propagation in free space is about one foot per nanosecond. So, in coaxial cable, the delay is around 1.4 nanoseconds per foot due to the slower propagation caused by the cable's dielectric constant. A 100-foot run introduces a delay of 140 nanoseconds. Fortunately, many clocks can compensate for that delay, so cable-induced time delay is seldom a degrading factor.

IRIG-B is easy to test in the laboratory and the field. Fig. 7 is an oscillogram taken from a digital oscilloscope showing the IRIG-B time-code outputs from three different satellite-synchronized clocks with respect to a trigger source from a precise standard.

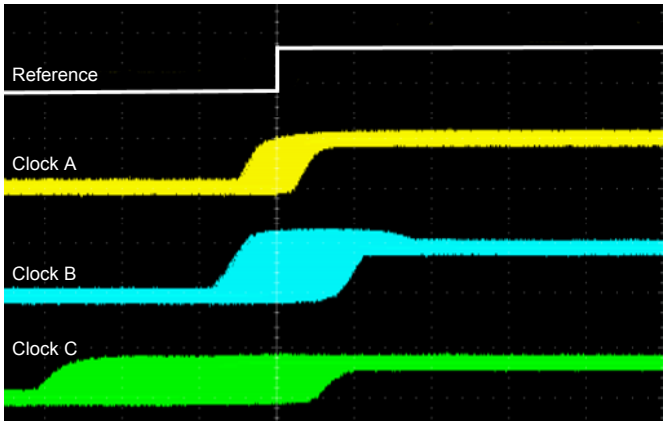

Fig. 7. IRIG-B time-code outputs captured from three satellite clocks.

Owing to the simplicity, versatility, economy, and accuracy of IRIG-B, this time code is still going strong after 55 years.

D. Network Time Protocol

Network Time Protocol (NTP) is a time synchronization protocol used over Ethernet networks. It is an integral part of modern networked systems and is used by virtually every computer connected to the Internet.

NTP uses a client-server model with clients querying the server approximately every 15 minutes. Because communications network topologies are not static, it is necessary to use statistical methods and averaging to obtain robust latency estimates between the time source and the client. Further, to enhance the reliability of time determination, NTP clients typically use multiple servers. A simplified version of the NTP protocol called Simple Network Time Protocol (SNTP) uses a single server and simple timing algorithms, thus lowering the client complexity while retaining reasonable accuracy on small networks. The accuracy of NTP and SNTP is usually in the order of milliseconds. This accuracy is sufficient for time tagging of oscillographic events and SCADA data but inadequate for more demanding power system applications such as synchrophasors, line differential protection, sampled values measurements, and time-domain protection.

E. Precision Time Protocol

Precision Time Protocol (PTP), also known as IEEE 1588, is a message-based time transfer protocol, optimized for Ethernet networks. The first version of the standard was released in 2002, with Version 2 following in 2008. Reference

[15] provides additional details about the standard. For the purposes of this paper, it is sufficient to know that PTP uses a ping-pong-type message exchange over an Ethernet network to distribute time from source to client devices. PTP exchanges messages for synchronizing client devices to sources once every second.

To achieve submicrosecond time synchronization accuracies using PTP, all the devices in the network (source clocks, switches, and the clients) must have hardware time stamping. Without hardware time stamping, PTP is no different than NTP in terms of accuracy. PTP enables, but does not guarantee, submicrosecond accuracies. To achieve submicrosecond accuracies with PTP, we must analyze the following network-specific characteristics:

- Delay variations that PTP messages experience in the network. To minimize these, we must deploy special PTP switches throughout the entire network.
- Communications path delay. This delay can be significant where PTP messages traverse multiple switches before reaching their destination. In order to compensate for delays through switches, a peer-to-peer delay mechanism is used.
- Network asymmetry. This can impact PTP accuracy if not properly characterized and understood.

For network-based time protocols like NTP and PTP, computer-based software programs, like Wireshark, are used to analyze the network traffic. Characterizing the performance of PTP for high-accuracy applications requires advanced testing instrumentation. The advanced characterization systems include emulating a PTP client in the test instrument, communicating with the PTP source (device under test), and computing the packet delay variation over many samples. Characterizing this packet delay variation over various network conditions with network elements (switches, routers, etc.) between the source device and the client is a very involved process requiring sophisticated test plans. As discussed previously, IRIG-B protocol can be characterized using a simple oscilloscope with an external trigger signal.

PTP protocol is still in the early adoption phase in the power system industry. As already mentioned, PTP requires that network devices be equipped with special purpose time-stamping hardware, making it difficult to deploy PTP in existing networks built without this capability.

F. Implications of the Technologies

Because we can now tell "what time it is" to an accuracy of, say, ten nanoseconds, we can start thinking about where electrical events happened to within ten feet. The authors believe such precise timing will enable the application of traveling-wave technology in distribution systems—even within power plants and substations and not just on long transmission lines.

Moving from milliseconds, through microseconds, and into nanoseconds is starting to open many doors for controlling, protecting, operating, and even understanding electric power systems.

V. Examining the Power System in Nanoseconds

A. Power System Network and Traveling Waves

We describe a traveling wave on a lossless line by using a second order differential equation [16] [17].

$$\frac{1}{LC}\frac{\partial^2 v}{\partial x^2} = \frac{\partial^2 v}{\partial t^2} \tag{5}$$

The general solution to this equation consists of forward and backward component functions.

$$\begin{aligned} v &= f_1(x - vt) + f_2(x + vt) \\ i &= \frac{1}{Z_c}[f_1(x - vt) + f_2(x + vt)] \end{aligned} \tag{6}$$

The characteristic impedance of the line relates current (6) to voltage, and it is defined as the ratio of line inductance to line capacitance.

$$Z_C = \sqrt{\frac{L}{C}} \tag{7}$$

The velocity of propagation is related to the inductance, L, in units of H/m and the capacitance, C, in units of F/m.

$$v = \frac{1}{\sqrt{LC}} \tag{8}$$

At any discontinuity, a component of the original signal is both propagated and reflected. The reflection coefficient for voltage at the sending end, where Z_S is the source impedance, is given by (9).

$$\rho_S^{(V)} = \frac{Z_S - Z_C}{Z_S + Z_C} \tag{9}$$

The reflection coefficient for voltage at the receiving end, where Z_R is the receiving end impedance, is given by (10).

$$\rho_R^{(V)} = \frac{Z_R - Z_C}{Z_R + Z_C} \tag{10}$$

The current always reflects with the opposite sign of the voltage.

$$\rho_S^{(I)} = -\rho_S^{(V)}, \qquad \rho_R^{(I)} = -\rho_R^{(V)} \tag{11}$$

These equations provide the fundamental theory for understanding how traveling waves propagate on transmission lines.

1) Steady-State Traveling Waves

Consider the idealized example system shown in Fig. 8, representing a single-phase two-wire transmission line and purely resistive load. The generator model includes a governor and voltage regulator.

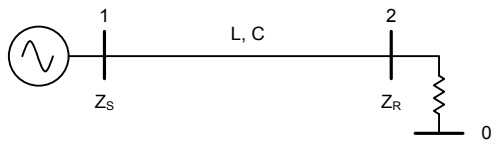

Fig. 8. Example system for traveling-wave analysis.

For simplicity of analysis, we set the line inductance to $\mathrm{L} = 1 \times 10^{-6}$ H/m and the line capacitance to $\mathrm{C} = 12 \times 10^{-12}$ F/m. In this case the velocity (8) is approximately equal to 288,675,135 m/s. As a fraction of the speed of light, c, this

equals $0.963 \times c$. For this example and with these values of inductance and capacitance, $Z_c = 289\ \Omega$.

During equilibrium conditions, a steady-state voltage profile develops across the line. This is shown in Fig. 8 for the case when $Z_S = \frac{1}{10} Z_C$ and $Z_R = \frac{2}{3} Z_C = 192.4\ \Omega$. By (10) and (11), $\rho_S^{(V)} = -0.82$ and $\rho_R^{(V)} = -0.2$.

In Fig. 9, the left plot shows the sending voltage waveform (marked as generator) as a function of time with per-unit scaling. The right plot shows the receiving voltage waveform (marked as load), also as a function of time and with per-unit scaling. The middle plot shows the voltage profile across the line at an instant in time as a function of the line distance. The total line length is set at one eighth of a wavelength. For $v = 0.963 \times c$, the line is 601.4 kilometers long. Notice how the voltage across the line connects the instantaneous voltage at the sending end and the instantaneous voltage at the receiving end. Fig. 10 shows the conditions at 2.0833 milliseconds (one eighth of a 60-cycle waveform) after the snapshot of time shown in Fig. 9.

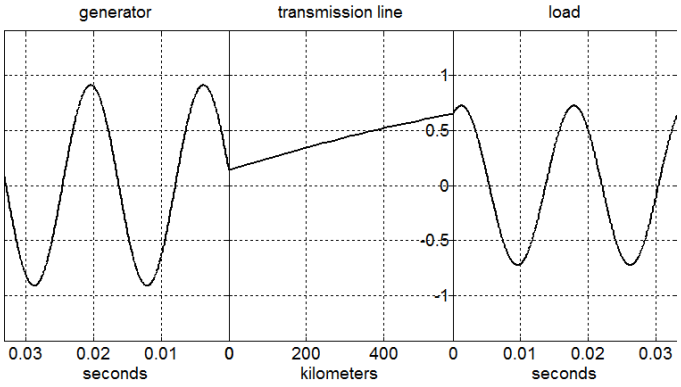

Fig. 9. Sinusoidal steady-state traveling wave across a transmission line.

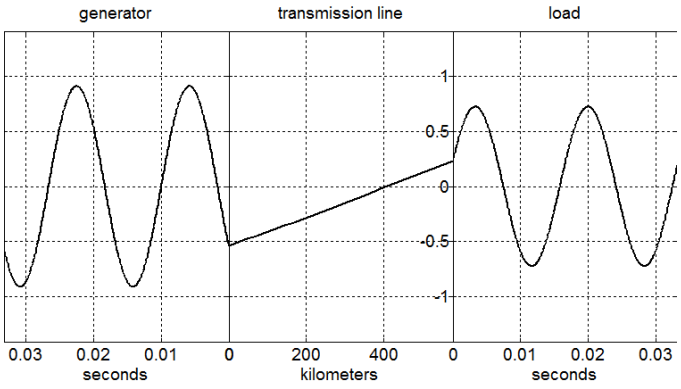

Fig. 10. Sinusoidal steady-state traveling wave across a transmission line 2.0833 milliseconds after the snapshot shown in Fig. 9.

The long-line form of the equilibrium equation for a transmission line gives the voltage across the line at equilibrium (capital letters in (12) denote the lack of time dependence). The propagation constant, γ, is a complex number because of the steady-state assumption that the sending voltage is a single frequency sinusoidal waveform.

$$V = \frac{1}{2}(V_R + I_R Z_C)e^{\gamma x} + \frac{1}{2}(V_R - I_R Z_C)e^{-\gamma x} \qquad (12)$$

In the case when $Z_R = Z_C$, the receiving voltage is $V_R = I_R Z_C$. In this case, the second term in (12) drops out and the first term becomes a function of V_R. There are no reflections on the line. It behaves as if the receiving end extends to infinity. This is the case of maximum power transfer. Also, for a lossless line $\gamma = j2\pi f\sqrt{LC}$ and (13) results.

$$V(x) = V_R e^{j2\pi f\sqrt{LC}x} \qquad (13)$$

Although these equations are constant with respect to time, Fig. 9 and Fig. 10 clearly show that the waveform on the line is quite dynamic. The steady-state conditions are with respect to properties of the waveform, not the waveform itself. The well-known steady-state equation (12) only applies for a pure sinusoid at a single frequency. The quasi-stationary approximation that is discussed in Section II is applicable when frequency variations, Δf, are changing more slowly in time than the propagation delay of the line. Therefore, both traveling-wave theory and steady-state theory give identical results for steady-state conditions. Under dynamic conditions, these assumptions no longer hold. The next sections describe line signal characteristics from the traveling-wave perspective.

2) Step Change in Load

Consider the case of a power system fault or a sudden step change in load. Fig. 11 shows the same steady-state condition as Fig. 9 with the addition of the current, shown in blue. The current reflection coefficients are opposite those of voltage and have multiple reflections that result in the phase shift at the source between current and voltage as shown in Fig. 11. With the phasor approximation, the phase shift is a result of the complex inductive and capacitive impedance. From a traveling-wave perspective, it is only due to reflections and time delays. The voltage and current of any given reflection, even the components of sinusoidal signals, are always related by (7), from a traveling-wave perspective.

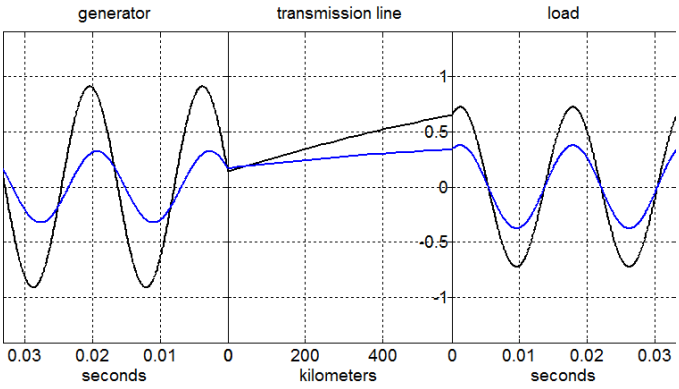

Fig. 11. Steady-state voltage (black) case of Fig. 9, with the addition of current waveforms (blue), as traveling waves.

For ease of visibility, we apply a step increase of 25 percent at the load. This induces a traveling wave that propagates from the load to the generator, as shown in Fig. 12 through Fig. 14. The phase angle increases at the sending end because the increase in load brings it further from matching the line impedance.

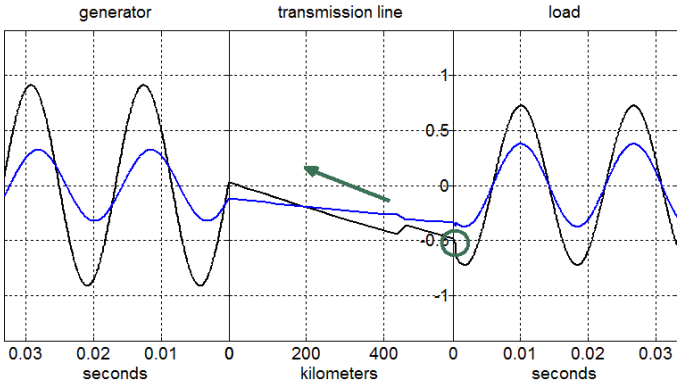

Fig. 12. Load-step-induced traveling wave riding on top of the sinusoidal traveling waves. The portion of the wave circled in green shows the change in signal as a result of the step change in load.

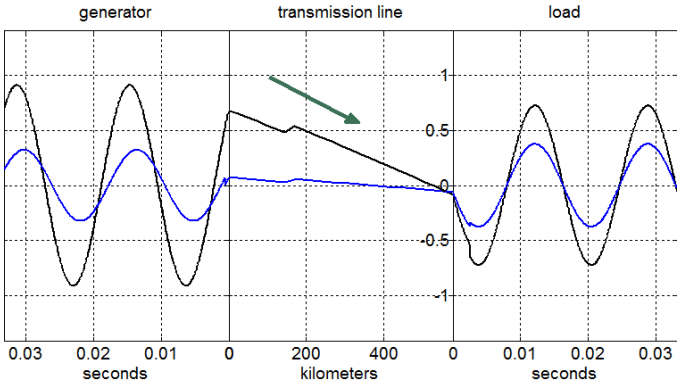

Fig. 13. Load-step-induced traveling wave 2.0833 milliseconds after the snapshot shown in Fig. 12.

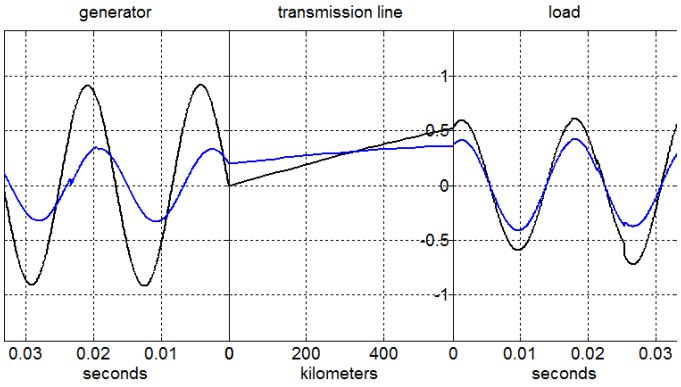

Fig. 14. New sinusoidal steady-state traveling waves.

The generator at the sending end is unable to receive information about the load change until the traveling wave crosses the transmission line. For this example, with a long line, the transient propagation time is 2.0833 milliseconds. For the step change in load, as the wave propagates, it creates a simultaneous propagation of power. Fig. 15 shows the same conditions of Fig. 12 with the addition of the power across the line, shown in red.

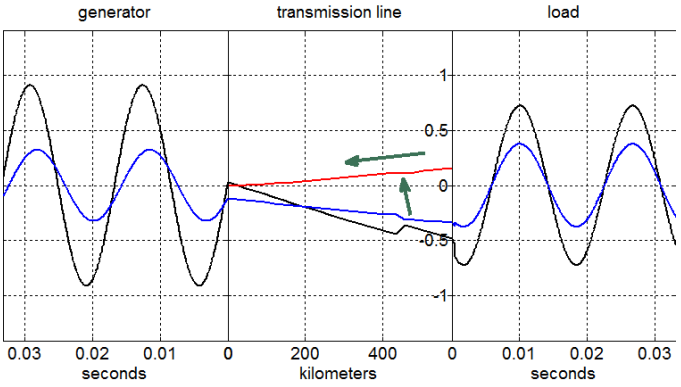

Fig. 15. Traveling power wave. The red line is power and the change in power travels with the voltage and current traveling wave.

3) Disconnection of Generation

To understand and visualize the dynamic energy stored in the line, we disconnect the source. A traveling wave propagates from the source toward the load as shown in Fig. 16.

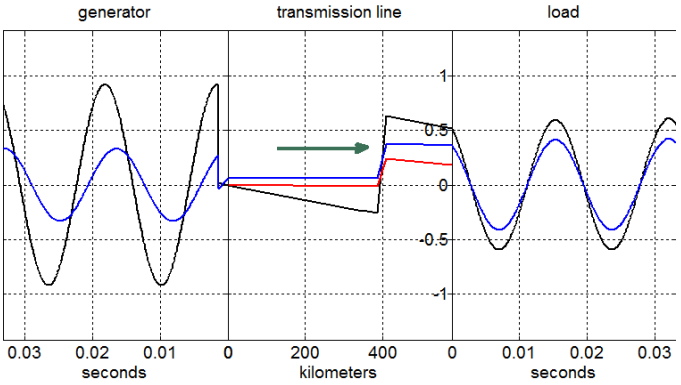

Fig. 16. Traveling wave of disturbance propagating toward the load after disconnecting the source.

The load operates without any knowledge of the source change for a full 2.0833 milliseconds. All energy required by the load is supplied by the line.

B. Response of Generation to Load Change

Returning to the example of a step change in load, the response of the system happens at multiple time scales. Each scale requires a different level of time accuracy and modeling for applications analyzing or controlling dynamics of the power system at that scale. Generally there are five sets of differential equations.

$$\begin{aligned} \dot{\underline{u}} &= \underline{p}\left(\underline{u},\underline{z},\underline{y},\underline{x},\underline{w}\right) \\ \dot{\underline{z}} &= \underline{q}\left(\underline{u},\underline{z},\underline{y},\underline{x},\underline{w}\right) \\ \dot{\underline{y}} &= \underline{g}\left(\underline{u},\underline{z},\underline{y},\underline{x},\underline{w}\right) \\ \dot{\underline{x}} &= \underline{f}\left(\underline{u},\underline{z},\underline{y},\underline{x},\underline{w}\right) \\ \dot{\underline{w}} &= \underline{h}\left(\underline{u},\underline{z},\underline{y},\underline{x},\underline{w}\right) \end{aligned} \tag{14}$$

- $\dot{\underline{u}} = \underline{p}()$ are a set of traveling-wave equations from (5) that are separated into first order differential equations. The variables are traveling-wave voltages and currents.
- $\dot{\underline{z}} = \underline{q}()$ are passive RLC differential equations. The variables are time-domain voltages and currents.

- $\underline{\dot{y}} = \underline{g}()$ are quasi-stationary phasor equations relating to the power system network. The state variables are voltages and currents as phasors.
- $\underline{\dot{x}} = \underline{f}()$ are electromechanical equations. Examples of the state variables include rotor fields, automatic voltage regulation controllers, and governors. Also at this level of detail are power electronic controllers.
- $\underline{\dot{w}} = \underline{h}()$ are slow local and wide-area control equations. The state variables include transformer tap change values, load values, and generation set values.

Table II provides filtering characteristics for the first three sets of equations in (14): time domain, passive RLC, and phasors. For processing, the analysis and control filtering requirements are different for each. In the time-domain traveling wave, the high-frequency components are important. The sample rate can be millions of samples per second. Passive RLC-related characteristics use wide-band filtering and are sampled in thousands of samples per second. Phasor filtering enforces the quasi-stationary restriction. Therefore, the filtering is typically bandpass around the nominal system frequency. The sample rate for synchrophasors is in the one-sample-per-cycle range.

TABLE II
FILTERING CHARACTERISTICS

	Time Domain	**Passive RLC**	**Phasors**
Example Equation	(5) – (11)	$v_F = v - \left(Ri + L\frac{di}{dt}\right)$	$V_F = V - ZI$
Filtering	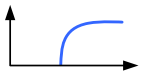	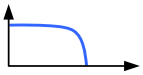	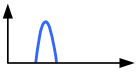
Sampling Rate (per second)	1,000,000	10,000	100

1) First 100 Nanoseconds: Initiating Traveling Wave

The system initially responds with a traveling wave, Fig. 12 through Fig. 14. Until the traveling wave reaches a junction, the remainder of the power system is unaware of any changes. All power changes required by the load are supplied by the transmission line. The time delay of a propagating wave from its source to a measuring device is given by (15), where the velocity, v, is given by (8).

$$t_{prop} = \frac{line\ length}{v} \tag{15}$$

2) Microseconds to Milliseconds: Reflected Traveling Wave

During the time of reflection, the disturbance radiates to the rest of the system. Modeling this phenomenon requires traveling wave equations (5) to (11).

3) Milliseconds: Passive RLC

The power system then acts as a linear RLC system. Loads are primarily a constant impedance during this time. The energy required by load changes is supplied by passive system storage. These changes are much faster than the response time of the electromechanical states, $\underline{x}$, or slow control states, $\underline{w}$.

$$\begin{aligned} \underline{\dot{z}} &= \underline{q}\left(\underline{z}, \underline{y}; \underline{x}, \underline{w}\right) \\ \underline{\dot{x}} &= \underline{0} \\ \underline{\dot{w}} &= \underline{0} \end{aligned} \tag{16}$$

4) Milliseconds to Seconds: Electromechanics

After RLC dynamics, the power system then responds as a set of differential algebraic equations (DAE). The network $\underline{y}$ is taken as instantaneously fast on this time-scale. Therefore, $\underline{0} = \underline{g}()$ meaning that these state variables track in equilibrium and become algebraic equations.

$$\begin{aligned} \underline{0} &= \underline{g}\left(\underline{y}, \underline{x}; \underline{w}\right) \\ \underline{\dot{x}} &= \underline{f}\left(\underline{y}, \underline{x}; \underline{w}\right) \\ \underline{\dot{w}} &= \underline{0} \end{aligned} \tag{17}$$

Note that the algebraic condition $\underline{0} = \underline{g}()$ can become unsolvable and lead to fast instability and power system collapse [18]. Local power system load and slow control state variables, are effectively fixed parameters for the network states, $\underline{y}$, and machine states, $\underline{x}$, as shown in (17). The generation loss response shown later in Fig. 17 demonstrates the electromechanical dynamics of the power system.

5) Seconds: Distributed Controls

Finally, the slower controls respond. Loads can be constant power or constant current. Instability can develop at this timescale if the controls constrained by either $\underline{0} = \underline{g}()$ or $\underline{0} = \underline{f}()$ are driven toward unstable regions.

$$\begin{aligned} \underline{0} &= \underline{g}\left(\underline{y}, \underline{x}, \underline{w}\right) \\ \underline{0} &= \underline{f}\left(\underline{y}, \underline{x}, \underline{w}\right) \\ \underline{\dot{w}} &= \underline{h}\left(\underline{y}, \underline{x}, \underline{w}\right) \end{aligned} \tag{18}$$

C. Energy Packets

Moving from a phasor-based approximation to a time-based measurement system can change the way we measure and analyze electric power. This section outlines the possibility of moving from a variable rate, average power analysis to a fixed rate, energy packet analysis approach.

1) Time Averaged Power

Electric power is traditionally separated into time-averaged real and reactive components. The time-averaged real component of power is defined as the integral of the product of instantaneous voltage and current.

$$P_{avg}(t_k) = \frac{1}{NT}\int_{t_k - NT}^{t_k} v(\sigma) i(\sigma) d\sigma \tag{19}$$

The integration in (19) is over an integer number, N, cycles, where T is given by (20) and ω_{line} is the measured line frequency. The average power measurement is available at time instant t_k, which varies as the measured line frequency varies.

$$T = {}^{2\pi}/_{\omega_{line}} \tag{20}$$

The integration of power results in energy. Average power (19) uses the energy integral but converts units back to power through the time varying normalization factor (20).

Several methods are available to calculate the reactive component of power. One is based on the power triangle relationship between apparent and real power. This calculation begins with the RMS quantities.

$$V_{RMS}(t_k) = \sqrt{\frac{1}{NT}\int_{t_k-NT}^{t_k} v(\sigma)^2 d\sigma}$$
$$I_{RMS}(t_k) = \sqrt{\frac{1}{NT}\int_{t_k-NT}^{t_k} i(\sigma)^2 d\sigma} \quad (21)$$

From the RMS quantities, compute reactive power with equation (22).

$$Q_{avg}(t_k) = \sqrt{\left(V_{RMS}(t_k)I_{RMS}(t_k)\right)^2 - P_{avg}(t_k)^2} \quad (22)$$

It is interesting to investigate how real and reactive power, calculated as described in (19) to (22), relate to time. As N increases, the accuracy of the measurements increase due to a longer averaging interval. However, a longer time is required until new power quantities are available. At a minimum, $N = 1$, and the calculation latency is equal to T.

The relationship in (20) between T and ω_{line} results in two complications. The first issue is that ω_{line} is not a directly measured quantity. It is estimated based on the instantaneous values of either voltage or current. Typically a filtered version of voltage is used for the estimate. In steady state, the estimate of ω_{line} is very accurate. However, during transient conditions, the estimate is dependent on the degree of pre-estimation filtering and the latency of the filtering compared to the rate of change of the frequency.

The second issue is that ω_{line} varies throughout the power system during transient conditions. The calculation latency is variable in length due to its dependence on ω_{line}, according to (20). Consider the step response of a typical power system shown in Fig. 17. This is the response of the North American Western Area on May 30, 2013 after the loss of generation totaling 2.5 gigawatts. The frequency is not constant throughout the power system during the disturbance. It varies by as much as 200 millihertz between two locations at the same instant in time. This makes comparison of power system quantities that are accurate in time difficult because, according to (20), the time it takes to calculate an estimated power quantity is variable.

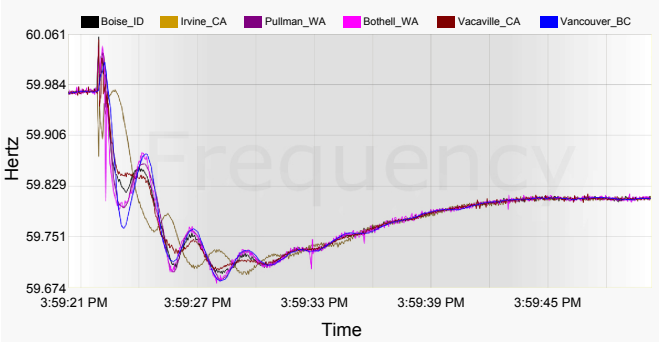

Fig. 17. Estimated frequency at various points in the power system.

2) Energy Packet Theory

Moving from a cycle-based phasor calculation to a time-based calculation results in a fixed processing latency and also eliminates the dependence of the measurement on ω_{line}. For time-based calculations, it is potentially preferable to operate with energy as the base unit. Indeed, energy is the physical characterization of the original integral (19), prior to scaling.

An energy packet, E_p, is defined here as the energy exchanged during the time interval $t_k - T'$ to t_k. The equation to compute an energy packet is given by (23). Although (23) initially appears similar to (19), note that there is no dependence on line frequency. The units of (23) are joules. The lower integration limit is initiated at a delay of T', which is a fixed constant and does not vary.

$$E_p(t_k) = \int_{t_k-T'}^{t_k} v(\sigma)i(\sigma)d\sigma \quad (23)$$

Consider the nominal case of steady-state voltage and current conditions across a transmission line (24). The voltage is labeled $v_S(t)$, with subscript "S" to indicate source.

$$v_S(t) = V_S cos(\omega t)$$
$$i(t) = Icos(\omega t - \phi) \quad (24)$$

The phase angle is the ratio of inductance to resistance, assuming an inductive transmission line and a resistive load.

$$\phi = tan^{-1}\left({}^{\omega L}/_{R}\right) \quad (25)$$

We prepare the integral in (23) for this case by first multiplying voltage by current and applying a few simple trigonometric identities.

$$E_S(t_k) = \frac{1}{2}V_S I \int_{t_k-T'}^{t_k} \left[cos\phi\left(1 + cos(2\omega\sigma)\right) + sin\phi sin(2\omega\sigma)\right] d\sigma \quad (26)$$

Next, we compute the energy packet integral and expand into common terms. This is the energy input to the circuit. The energy during half of the voltage input cycle results in creating a magnetic field at the inductor and dissipating heat in the resistor. For the other half of the cycle, the inductor returns its energy to the source and the resistor continues to dissipate heat.

$$E_S(t_k) = \frac{1}{2}V_S I \left\{ \begin{matrix} T'cos\phi \\ +\frac{cos\phi}{2\omega}\left[sin(2\omega t_k) - \sin(2\omega(t_k - T'))\right] \\ -\frac{sin\phi}{2\omega}\left[cos(2\omega t_k) - \cos(2\omega(t_k - T'))\right] \end{matrix} \right\} \quad (27)$$

At the receiving end of the line, the resistor current and voltage are in phase.

$$v_R(t) = V_R cos(\omega t - \phi)$$
$$i(t) = Icos(\omega t - \phi) \quad (28)$$

The energy packet at the receiver is given by the integral of the product of receive voltage and current.

$$E_R(t_k) = \frac{1}{2}V_S Icos\phi \int_{t_k-T'}^{t_k} \left[\begin{matrix} 1 + cos(2\phi)cos(2\omega\sigma) + \\ sin(2\phi)sin(2\omega\sigma) \end{matrix}\right] d\sigma \quad (29)$$

Next, compute the integral and then expand into common terms. At the receiving end, the energy is physically due to heat dissipation in the resistor.

$$E_R(t_k) = \frac{1}{2} V_S I cos\phi$$

$$\begin{Bmatrix} T' + \frac{cos\phi}{2\omega}\,[sin(2\omega t_k) - \sin(2\omega(t_k - T'))] \\ -\frac{sin\phi}{2\omega}\,[cos(2\omega t_k) - \cos(2\omega(t_k - T'))] \end{Bmatrix} \quad (30)$$

The sending energy packet in (27) and receiving energy packet in (30) differ by the energy transferred due to the inductor. Notice that when $T' = {}^{\pi}/_{\omega}$, the differences between (27) and (30) disappear, (31). This is because the average energy over a cycle is independent of the inductor. However, selecting this value for T' results in the same problems with measuring frequency and varying data intervals for time-averaged power (19).

$$E_S(t_k) = E_R(t_k) = \frac{1}{2} VIT' cos\phi \quad (31)$$

3) Energy Packets vs. KYZ

At this point, it is instructive to compare the implementation of time-averaged power (19) with energy packets (23). A common method of communicating time-averaged power is with either KZ pulses or KYZ pulses.

Fig. 18 shows a representation of power-flow with exaggerated variations along with associated KYZ pulses. The energy represented by each pulse is constant, and the information is contained in the time interval between pulses. This is a possible limitation of the method because many factors contribute to uncertainty in the interval between pulses. These include network delays due to equipment, network delays due to physical transmission time, and communication buffering. It is possible to apply a calibration step to remove systematic errors but such an approach is unable to remove variable errors. Dynamic calibration is possible but this is only accurate if latency variability is slower than the calibration update interval.

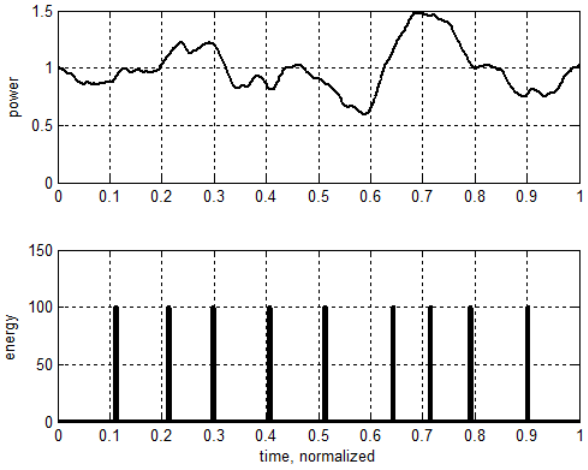

Fig. 18. Traditional KYZ pulses.

Fig. 19 shows an exaggerated power flow along with fixed-time-interval energy pulses. In this case, the energy represented in each packet of information varies but the time interval is constant. Including a time stamp with each measurement makes the information independent of network delays and other sources of variation in time intervals. Accuracy is limited only by the measuring devices. Controlling the accuracy of the measuring devices is a simpler engineering problem than trying to control the accuracy of an entire network.

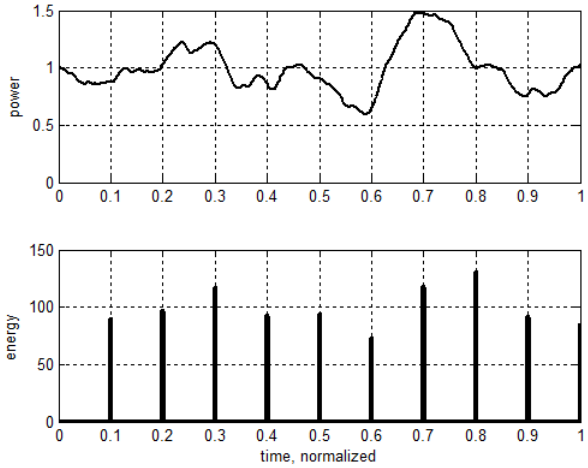

Fig. 19. Energy pulses and the fixed time intervals between packets.

The energy packet approach is an ongoing area of research. This section has served to highlight some of the potential benefits of energy packets along with some challenges they present.

VI. Conclusion

Power system monitoring and control has greatly benefited from the improvements in time accuracy and precision outlined in this paper. By moving from millisecond, to microsecond, and now to nanosecond precision, we are implementing and widely deploying new applications.

Time technology is not only more accurate and precise but it is also more reliable. Today, multiple time sources and time distribution methods, both local and wide area, are available. We have built robust and reliable timing systems that use a layered approach to provide precise and accurate time for power system applications.

With these advances in time technology, power system protection, analysis, and control is moving from the phasor domain to the time domain. Algorithms based on traveling waves result in faster response time and more accurate fault locating.

Wide-area analysis of electric power phenomena is not limited by phasors. System monitoring and modeling now take advantage of the full range of electrical dynamics, from those happening at the millisecond scale to those happening at the nanosecond scale. Energy packets are enabling measurements based on consistent time intervals.

Nanosecond time is available today and provides us with new insight into electric power systems.

VII. References

[1] W. Schossig, "Generations of Protection–The Beginning of Electromechanical Distance Protection," PAC World, December 2012.

[2] F. C. Schweppe; J. Wildes, "Power System Static-State Estimation, Part I: Exact Model," *IEEE Trans. Power App. Syst.*, vol. PAS-89, pp. 120–125, Jan. 1970.

[3] M. Ando, E. O. Schweitzer, III, and R. A. Baker, "Development and Field-Data Evaluation of Single-End Fault Locator for Two-Terminal HVDC Transmission Lines, Part II: Algorithm and Evaluation," *IEEE*

Transactions on Power Apparatus and Systems, Vol. PAS–104, Issue 12, December 1985, pp. 3531–3537.

[4] E. Martinez, N. Juárez, A. Guzmán, G. Zweigle, J. León, "Using Synchronized Phasor Angle Difference for Wide-Area Protection and Control," proceedings of the 33rd Annual Western Protective Relay Conference, Spokane, WA, October 2006.

[5] E. O. Schweitzer, III, and D. E. Whitehead, "Real-world Synchrophasor Solutions," proceedings of the 35th Annual Western Protective Relay Conference, Spokane, WA, October 2008.

[6] G. Zweigle, "A Wide-Area, Wide-Spectrum Big Data System," IEEE General Meeting, Denver, Colorado, July 26–30, 2015.

[7] E. O. Schweitzer, III, A. Guzmán, M. V. Mynam, V. Skendzic, B. Kasztenny, and S. Marx, "Locating Faults by the Traveling Waves They Launch," proceedings of the 40th Annual Western Protective Relay Conference, Spokane, WA, October 2013.

[8] M. Ilic, J. Zaborszky, *Dynamics and Control of Large Electric Power Systems*, John Wiley and Sons, Inc. 2000.

[9] B. Kasztenny, N. Fischer, K. Fodero, and A. Zvarych, "Communications and Data Synchronization for Line Current Differential Scheme," proceedings of the 38th Annual Western Protective Relay Conference, Spokane, WA, October 2011.

[10] V. Skendzic, I. Ender, and G. Zweigle, "IEC 61850-9-2 Process Bus and Its Impact on Power System Protection and Control Reliability," proceedings of the 9th Annual Western Power Delivery Automation Conference, Spokane, WA, April 2007.

[11] IEC 61850-9-2:2011, Communication Networks and Systems in Substations – Part 9-2: Specific Communication System mapping (SCSM) – Sampled Values Over ISO/IEC 802-3, Edition 2.0, September 2011.

[12] IEC TR 61850-90-5:2012, Communication Networks and Systems in Substations – Part 90-5: Use of IEC 61850 to transmit synchrophasor information according to IEEE C37.118, Edition 1.0, May 2012.

[13] S. Achanta, S. T. Watt, E. Sagen, "Mitigating GPS Vulnerabilities," proceedings of the 17th Annual Power and Energy Automation Conference, Spokane, WA, March 2015.

[14] E. O. Schweitzer, III, D. Whitehead, K. Fodero, and P. Robertson, "Merging SONET and Ethernet Communications for Power System Applications," proceedings of the 38th Annual Western Protective Relay Conference, Spokane, WA, October 2011.

[15] S. T. Watt, S Achanta, H. Abubakari, E. Sagen; "Understanding and Applying Precision Time Protocol," proceedings of the 16th Annual Power and Energy Automation Conference, Spokane, Washington, March 2014.

[16] L.V. Bewley, Traveling Waves on Transmission Systems, Dover Publications, Inc., New York, 1933.

[17] W. D. Stevenson, Jr. Elements of Power System Analysis, McGraw-Hill, 1982.

[18] V. Venkatasubramanian, H. Schattler, and J. Zaborszky, "Global Voltage Dynamics: Study of a Generator with Voltage Control, Transmission and Matched MW Load," proceedings of the 29th IEEE Conference on Decision and Control, Honolulu, HI, December 1990, pp. 3045-3056.

VIII. BIOGRAPHIES

Dr. Edmund O. Schweitzer, III is recognized as a pioneer in digital protection and holds the grade of Fellow in the IEEE, a title bestowed on less than one percent of IEEE members. In 2002, he was elected as a member of the National Academy of Engineering. Dr. Schweitzer received the 2012 Medal in Power Engineering, the highest award given by IEEE, for his leadership in revolutionizing the performance of electrical power systems with computer-based protection and control equipment. Dr. Schweitzer is the recipient of the Regents' Distinguished Alumnus Award and Graduate Alumni Achievement Award from Washington State University and the Purdue University Outstanding Electrical and Computer Engineer Award. He has also been awarded honorary doctorates from both the Universidad Autónoma de Nuevo León, in Monterrey, Mexico, and the Universidad Autónoma de San Luis Potosí, in San Luis Potosí, Mexico, for his contributions to the development of electric power systems worldwide. He has written dozens of technical papers in the areas of digital relay design and reliability, and holds nearly 200 patents worldwide pertaining to electric power system protection, metering, monitoring, and control. Dr. Schweitzer received his bachelor's and master's degrees in electrical engineering from Purdue University, and his doctorate from Washington State University. He served on the electrical engineering faculties of Ohio University and Washington State University, and in 1982, he founded Schweitzer Engineering Laboratories, Inc. to develop and manufacture digital protective relays and related products and services.

David E. Whitehead, P.E., is the vice president of research and development at Schweitzer Engineering Laboratories, Inc. (SEL) and also oversees SEL's government services division. He is a member of the SEL Board of Directors. Mr. Whitehead joined SEL in 1994 and has held the positions of hardware engineer, research engineer, and chief engineer of the government services division. Prior to joining SEL, Mr. Whitehead worked for General Dynamics, Electric Boat Division as a combat systems engineer. He received his BSEE from Washington State University in 1989 and his MSEE from Rensselaer Polytechnic Institute in 1994. He is a registered Professional Engineer in Washington, New York, and North Carolina. Mr. Whitehead is a senior member of the IEEE and also chairs the Power and Energy Society Substations C6 group that addresses serial cryptographic protocols. Mr. Whitehead currently holds 49 patents worldwide with several others pending.

Greg Zweigle serves as a Schweitzer Engineering Laboratories, Inc. fellow engineer and leads a research team and software development department. He holds a Ph.D. in electrical engineering and computer science, a master of science degree in (physical) chemistry, and a master of science degree in electrical engineering from Washington State University. He also has a bachelor of science degree in physics from Northwest Nazarene University. Zweigle is a senior member of the IEEE.

Veselin Skendzic is a principal research engineer at Schweitzer Engineering Laboratories, Inc. He earned his BS in electrical engineering from FESB, University of Split, Croatia; his Masters of Science from ETF, Zagreb, Croatia; and his Ph.D. from Texas A&M University, College Station, Texas. He has more than 25 years of experience in electronic circuit design and power system protection-related problems. He is a senior member of IEEE, has written multiple technical papers, and is actively contributing to IEEE and IEC standard development. He is a member of the IEEE Power Engineering Society (PES) and the IEEE Power System Relaying Committee (PSRC) and a past chair of the PSRC Relay Communications Subcommittee (H).

Shankar V. Achanta received his M.S. in electrical engineering from Arizona State University in 2002. He joined Schweitzer Engineering Laboratories, Inc. (SEL) in 2002 as a hardware engineer, developing electronics for communications devices, data acquisition circuits, and switch mode power supplies. Shankar currently holds three SEL patents, and he is an inventor on several patents that are pending in the field of precise timing and wireless communications. He currently holds the position of research and development manager for the precise time and wireless communications group at SEL.